Compact Modeling and Experimental Verification of Substrate Resistance in Lightly Doped Substrates

Hai Lan
Center for Integrated Systems
Stanford University
Stanford, CA 94305, USA
hailan@gloworm.stanford.edu

Tze Wee Chen
Center for Integrated Systems
Stanford University
Stanford, CA 94305, USA
tzewee@stanford.edu

Chi On Chui
Center for Integrated Systems
Stanford University
Stanford, CA 94305, USA
chion@stanford.edu

Robert W. Dutton
Center for Integrated Systems
Stanford University
Stanford, CA 94305, USA
rdutton@gloworm.stanford.edu

Abstract- This paper presents a synthesized compact modeling methodology for substrate noise coupling in a lightly doped silicon substrate process. Rigorous 3-D device simulations reveal the distinctive decaying trend of noise coupling in far field and near field regions. A new compact, scalable model is proposed to accommodate both far field and near field effects as well as contact size, perimeter, area, and separation of contacts. A test chip in a lightly doped P-type substrate, consisting of various combinations of substrate noise coupling configurations, is fabricated and tested. The proposed compact model is validated by the measurement data from the test chip.

I. Introduction

Design of mixed-signal integrated circuits and system-on-a-chip (SOC) has continued to be challenged by the substrate noise coupling issue. Due to the lossy nature of the common substrate, noise generated by the noisy digital circuitry can be easily injected into and propagate through the entire silicon substrate and eventually affect the sensitive analog and RF circuitry in several ways. In order to include substrate noise coupling effects into the design flow, proper substrate modeling is needed. Considerable research efforts have been put to characterize and model the substrate for noise analysis.

There are two major schools of methodology for modeling substrate, namely, 3-D mesh-based method and compact modeling method. The first method relies on fine 3-D grid meshing schemes to discretize the entire substrate in order to solve Poisson and continuity equations, quasi-static Laplace equations, or full-wave Maxwell equations [1], [2], [3], [4]. It is accurate however computationally expensive and thus is usually limited to simple configurations. The second method seeks macro models in scalable form [5], [6]. Its advantage of fast generation of substrate model potentially enables practical and efficient full-chip substrate noise analysis.

A comprehensive geometry-dependent macro model for substrate coupling in heavily doped substrate with a lightly doped epitaxial layer has been reported in [6]. Based on that work, an improved modeling including the near field effect has been proposed, which results in better substrate noise modeling for epitaxial silicon processes and enables substrate noise-aware layout synthesis [7]. While this work focuses on modeling substrate in epitaxial processes, lightly doped substrate is more widely used in CMOS or BiCMOS processes for analog, RF and mixed-signal ICs. A close-form resistance model is proposed to model the substrate coupling in lightly doped processes [5]. However, their model requires geometry-dependent fitting coefficients and thus can not be applied to a wide range of geometry combinations of contact structures.

A preferred model should be scalable in substrate contact geometry with a limited set of process-dependent fitting coefficients. In this paper, a synthesized compact modeling methodology of this kind for substrate resistance in lightly doped process is proposed and validated by the measurement from a test chip fabricated in a lightly doped process.

This paper is organized as follows. In Section II, 3-D device simulation results are discussed to reveal the substrate coupling decaying trend in near field and far field region. The modeling approach is then proposed. Section III details the test chip, including the customized lightly doped process and the arrays of test structures. It is followed in Section IV by the report of measurement data obtained from the test chip and the comparisons of the proposed model and the measurement results. Finally, conclusions are presented in Section V.

II. Modeling Approach

A. Near Field and Far Field Implication

It is generally true that substrate coupling resistance between two contacts increases as the separation increases. However, this general trend is manifest differently in the far field and near field regions. When the separation is large enough compared to contact size, both contacts see each other as a point. By contrast, when two contacts are close enough to each other, more significant spreading coupling effects are essential. Hence, the shape, size, and relative position all

contribute to the overall coupling. Fig. 1 qualitatively illustrates the far field and near field effects.

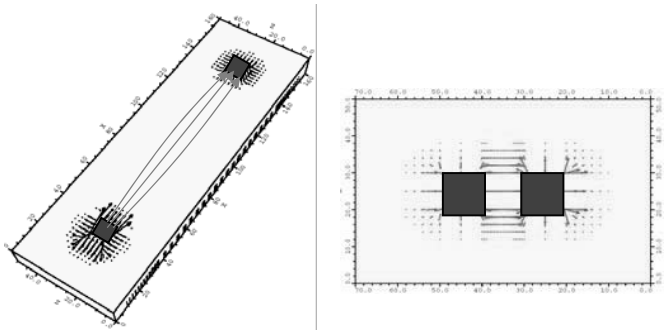

(a) (b)

Fig. 1. (a)Far field region: point to point lumping; (b)Near field region: more spreading coupling effects

Fig. 2 shows 3-D device simulation results for the substrate coupling resistance versus the separation in a lightly doped silicon substrate using the DAVINCI simulator [8]. The curve shown in the figure indicates different decay trends of noise coupling strength in near field and far field regions. As can be seen from the figure, while in the far field region it changes linearly with varying separation, in the near field region the substrate resistance decreases faster than linear fashion to approach zero resistance value as the separation decreases to zero.

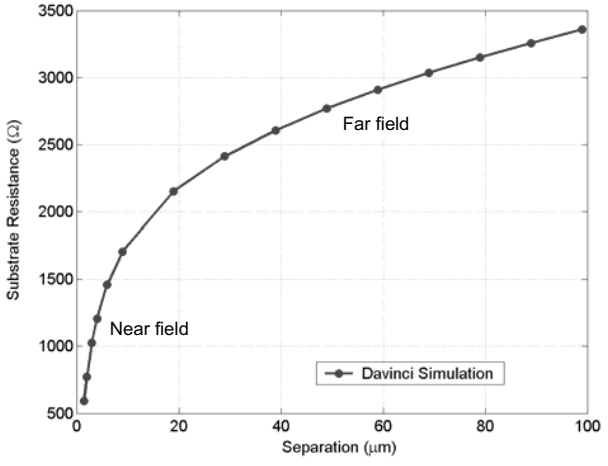

Fig. 2. Device simulation result indicating different characteristics in far field and near field

B. Definition of Distance: Geometric Mean Distance

The scalable model parameterization needs a proper definition of spacing, distance, or separation. Edge to edge distance is often used when two contacts are well aligned and thus the regular definition of distance is clear. However, this is not the case in general. When two contacts are not aligned and are not far away from each other, the regular definition of distance becomes somewhat ambiguous. Hence, a more appropriate and generic definition of distance needs to be introduced so that this geometrical parameter can be included in the compact model. For this purpose, the concept of Geometric Mean Distance (GMD) is used here. Fig. 3 shows a configuration of two rectangular contacts. The distance in the GMD sense, d_{GMD}, is defined as

$$d_{GMD} = \frac{\int_{L_2}\int_{W_2}\int_{L_1}\int_{W_1} r \cdot dx_1 \cdot dy_1 \cdot dx_2 \cdot dy_2}{W_1 \cdot L_1 \cdot W_2 \cdot L_2} \qquad (1)$$

where r is the distance between point (x_1, y_1) and point (x_2, y_2), W_1 and W_2 are the widths of two contacts, and L_1 and L_2 are the lengths of two contacts. GMD has been used in inductance computation for a long time [9]. By definition, it takes into account the area, perimeter, and relative position of two contacts. This is also a favorable property for the development of compact models for substrate resistance. The formula in (1) can be further simplified by various approximating closed-form expressions [9].

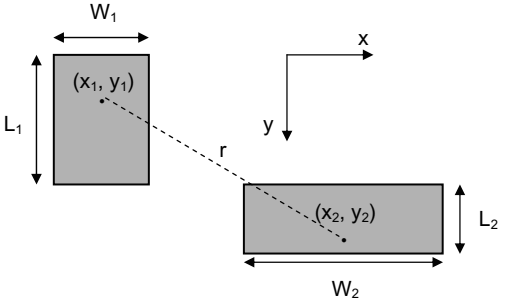

Fig. 3. Illustration of Geometric Mean Distance (GMD)

C. Synthesized Compact Model of Substrate Resistance

Based on the observation and device simulation discussed above, the proposed compact model of substrate coupling resistance between two arbitrarily sized contacts reads

$$R_{ij} = \beta \cdot [\ln(d_{ij} + 1)]^{\alpha_1} \cdot (s_i + s_j)^{\alpha_2} \cdot (p_i + p_j)^{\alpha_3} \qquad (2)$$

where d_{ij} is the geometric mean distance between two contacts, s_i and s_j are the areas of contact i and contact j, p_i and p_j are the perimeters of contact i and contact j. β,

α_1, α_2 and α_3 are four fitting coefficients, characterizing the substrate coupling resistance dependence on substrate doping profiles, separation between two contacts, contact areas, and contact perimeters, respectively. It is worth emphasizing that these fitting coefficients do not depend on contact geometry and in fact they are only process-dependent. They can be extracted by fitting the model above to rigorous device or electromagnetic simulation results or measurement data for a limited number of benchmarking substrate contact structures.

III. TEST CHIP

Fig. 4 shows the layout view of the test chip. The chip consists of 1200 sets of contact structures organized in seven arrays. The test pattern features P+ substrate contacts, N wells, N well contacts, and P+ guard rings of various combinations of sizes, perimeters, distances, and positions of aggressor-victim pairs relative to guard rings. It includes DC probe pads to support on-chip DC probing and G-S-G probe pads to facilitate high frequency S-parameter measurement.

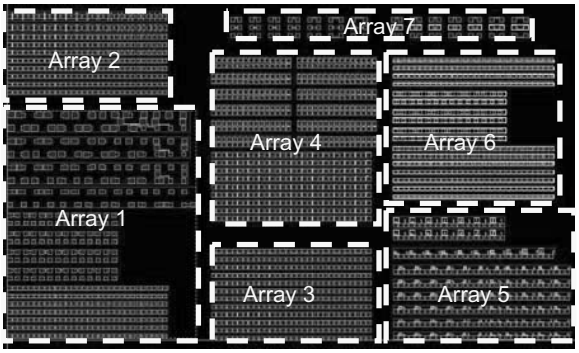

Fig. 4. Layout of the test chips, showing the test pattern organized in seven arrays

Fig. 5 illustrates the cross sectional schematic view of the substrate structure used for this test chip. A customized lightly doped silicon substrate process was developed. The process simulation TSUPREM [10] shows the doping profiles of P+ diffusion, P- bulk silicon, N+ well contact diffusion, and N well, etc. Fig. 6(a) shows that the bulk silicon is uniformly doped at $N_a=1\times10^{15}$ cm^{-3}. Fig. 6(b) shows that the N well depth is 1 μm with a peak concentration of $N_d=1\times10^{15}$ cm^{-3}.

The chip was fabricated using the Stanford Nano-Fabrication (SNF) facility. Fig. 7 shows the die photo of test chip and micro photographs of a few sampled regions on the chip.

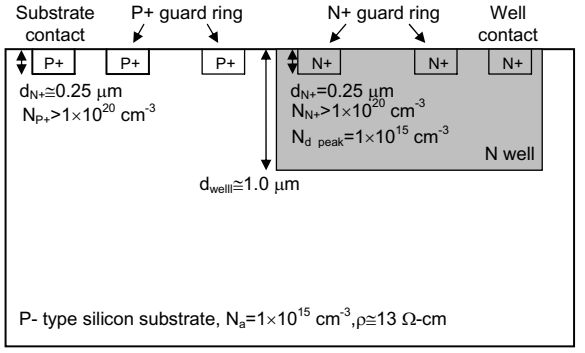

Fig. 5. Cross-section of the lightly doped silicon process used to fabricate the test chip

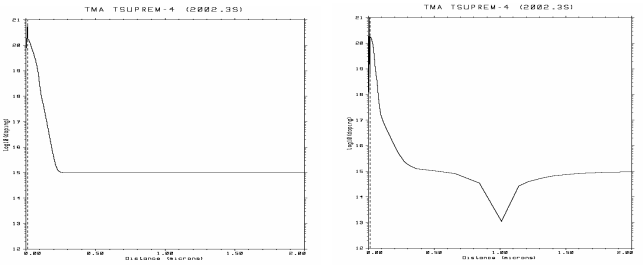

Fig. 6 Substrate doping profiles of the customized lightly doped silicon process: (a) P+ and P- bulk; (b)N+, N well and P- bulk

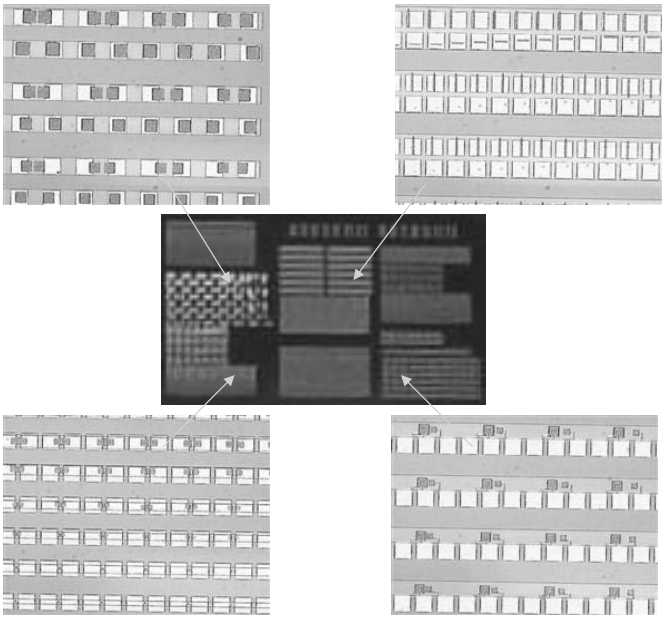

Fig. 7. Die photo of test chip (center) and magnified microphotographs of four sampled regions

IV. MEASUREMENT

Measurements were made using an on-chip probe station Cascade and HP semiconductor parameter analyzer. For all the test structures in Array 1 to 6, only DC probing was performed. Only the measurement of test structures in Array 7 involves high frequency characterization. However, since this paper only focuses on the substrate resistance modeling, the high frequency measurement is not reported here and will be reported in a later phase to calibrate the work in [11]. Fig. 8 shows the measurement setup for DC probing.

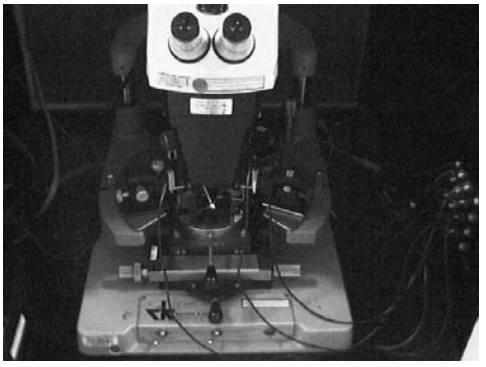

Fig. 8. Measurement setup

A. *Array 1: Square Contact to Square Contact*

This array consists of many pairs of square-shaped P+ type substrate contacts with various side widths and separations. The active sizes of contact vary from 1 by 1 to 20 by 20, where one unit corresponds to a physical length of 6 µm in active area. The separations between two contacts vary from 1.5 µm to as large as 400 µm. It should be pointed out here that it is the relative ratio of contact size to separation that matters from a near field and far field perspective.

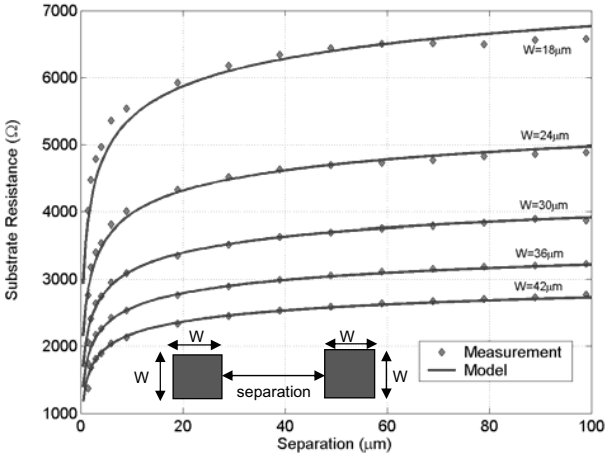

(a) Contact side width W=18, 24, 30, 36, and 42 µm

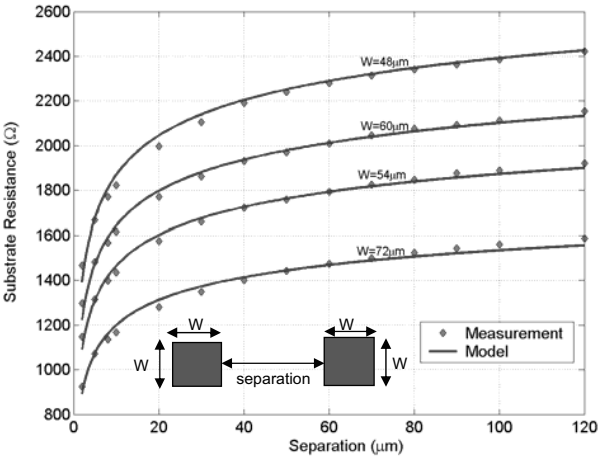

(b) Contact side width W=48, 60, 54, and 72 µm

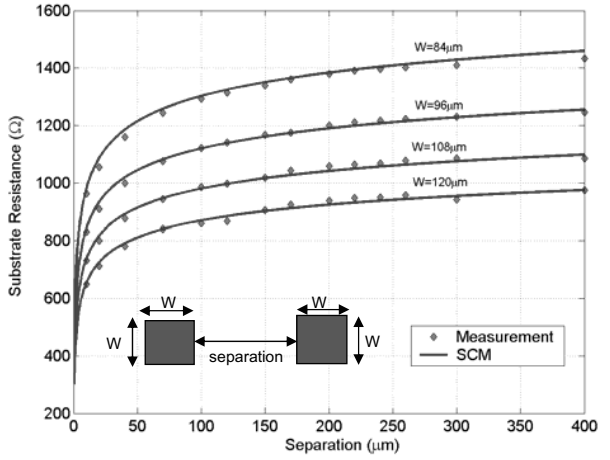

(c) Contact side width W= 84, 96, 108 and 120 µm

Fig. 9. Measurement data and modeling results of substrate resistance for test structures in Array 1, namely, square contact to square contact

Fig. 9 shows the comparison between measurement data and modeling results for sampled test structures in this array. In Fig. 9(a), the curves and data points corresponds to the decaying trend of the substrate coupling strength between square contact to square contact as the separation increases for different size of contacts, namely, W=18, 24, 30, 36 and 42 µm. Similarly, Fig. 9(b) shows the cases of W=48, 60, 54, and 72 µm and Fig. 9(c) shows the cases of W=84, 96, 108 and 120 µm. In all the cases, the compact model predictions, i.e., using Eq. (2), agree with the measurement data with relative error of less than 4%. This model consistently works well in both near field and far field regions.

Notice that the resistance decreases as the contact size increases and the resistance increases as the separation increases for each case. More importantly, as can be seen from these plots, all the coupling resistance exhibits a similar behavior: increasing more than linearly for relatively smaller separations and continuing to increase in a steady linear

fashion for relatively larger separations. Again, this observation confirms the near field and far field effects. The turning point between far field and near field is about 20~30 µm, 50~60 µm, and 90~100 µm for cases shown in Fig 9(a), (b), and (c), respectively. Although not precise, the turning point is about at the spacing equivalent to the size of contact itself. This can be used as a rule of thumb.

B. *Array 2: Rectangular Contact to Rectangular Contact*

Non-square shape rectangular contact structures are included in this array. The active lengths of contact vary from 1 to 25 units while the active width fixed at 1 unit.

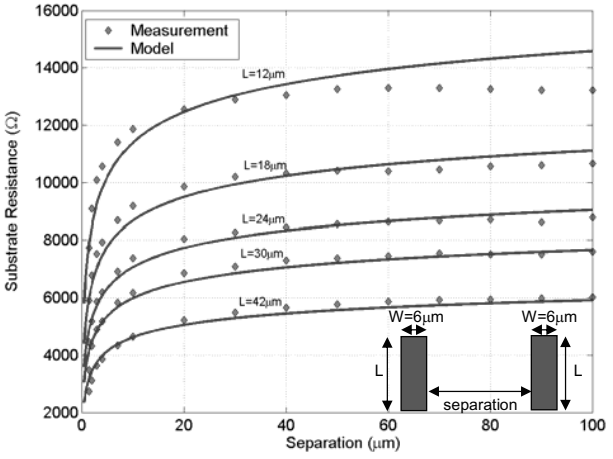

(a) Contact length L=12, 18, 24, 30 and 42 µm

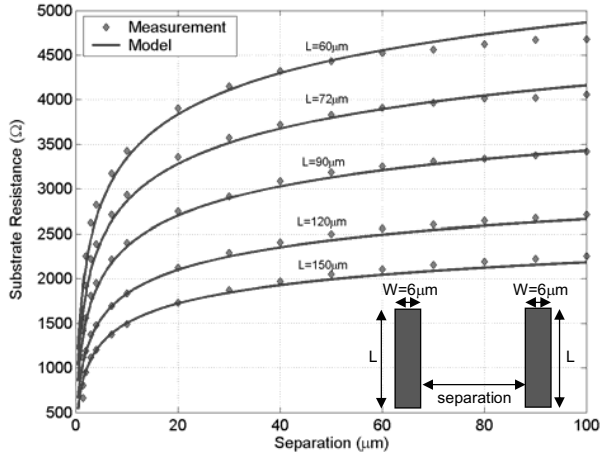

(b) Contact length L=60, 72, 90, 120 and 150 µm

Fig. 10. Measurement and modeling results of substrate resistance for test structures in Array 2, namely, rectangular contact to rectangular contact

Fig. 10 shows the measurement data and the model predictions. Results from the contacts with relative smaller lengths L=12, 18, 24, 30 and 42 µm are shown in Fig. 10(a). The cases of larger lengths L=60, 72, 90, 120 and 150 µm are shown in Fig. 10(b). In general the modeling results agree with the measurement data within 5% error. However, larger errors as high as 8% do occur in a few cases, typically when the substrate resistance is very high due to small active area and for large separations. It should be pointed out that even for these cases the model still works well in the near field region, with error less than 5%.

C. *Array 3: Arbitrarily Sized Contact Pairs*

In this array, the contact pairs in different geometry combination are studied. The comparisons of the results predicted by the model and the measurement data are shown in Fig. 11(a) and (b) for sampled test structures. The model consistently gives accurate resistance values compared to the measurement data. Typical error falls within 5% with only a few exceptions where the error goes as high as 10%.

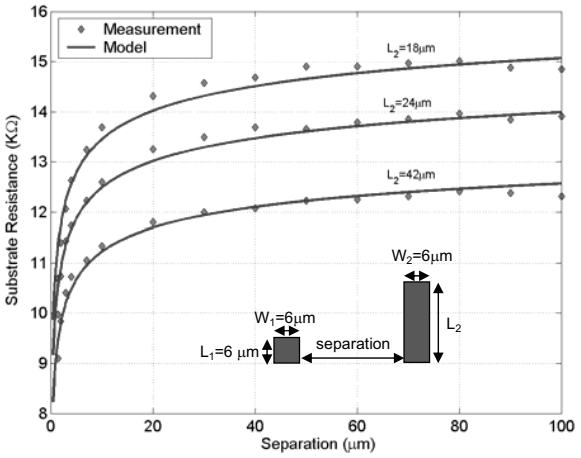

(a) W_1=6 µm, L_1=6 µm, W_2=6µm, and L_2=18, 24, 42 µm

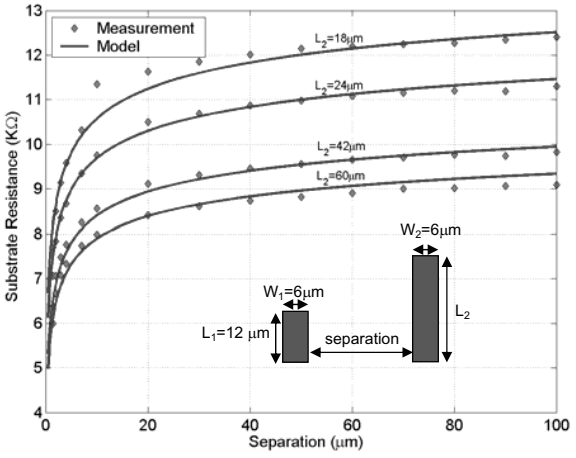

(b) W_1=6 µm, L_1=12 µm, W_2=6µm, L_2=18, 24, 42, and 60 µm

Fig. 11. Measurement and modeling results of substrate resistance for sampled test structures in Array 3

D. Array 4: Contacts Unaligned with Offset or Super Offset

To study the practical situation where two contacts are arbitrarily positioned, the test structures of contacts unaligned to each other with offset and super offset are included in this array.

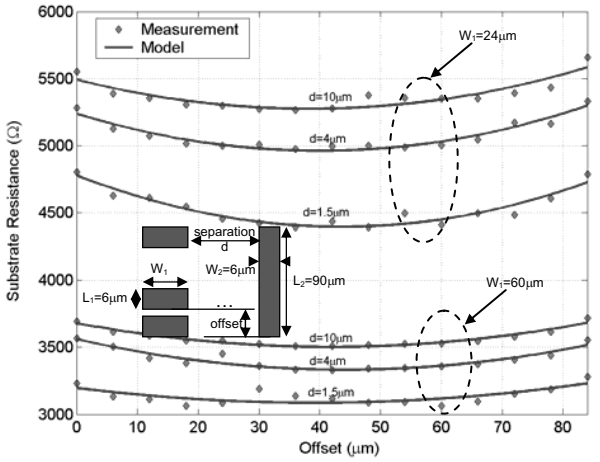

Fig. 12. Contacts Unaligned with Offset

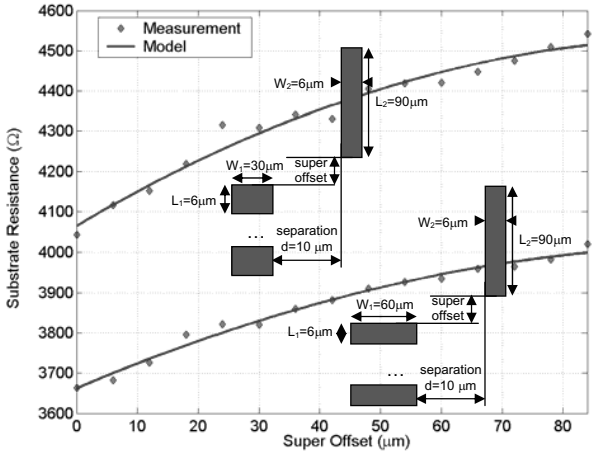

Fig. 13. Contacts Unaligned with Super Offset

The configuration of two contacts unaligned with each other is depicted in Fig. 12. The right contact is fixed in position and sized at 6 μm by 90 μm. The left contact is unaligned to the first one with an offset varying from 0 to 84 μm and sized at 6 μm by W_1. The measurement data and modeling results are also shown in the same figure. The upper and lower set of curves and data correspond to W_1=24 μm and W_1=60 μm, respectively. The plots clearly show that the noise coupling between these two contacts increases as the separation decreases or as the sensing area increases. They also show that the strongest coupling occurs when the left contact is center aligned with the right contact. Meanwhile, the coupling resistance increases by 10% when the left contact moves towards either end of the right contact for this particular layout.

Fig. 13 illustrates the configuration of two contacts unaligned with even more offset, namely, "super offset", as defined in the figure. Two different layouts with geometries labeled are shown there. The measurement data and the predicted results are drawn in the same figure, accompanied by the corresponding layout aside. Again, the model agrees with measurement data well. It is worth mentioning that the geometric mean distance concept was used here to avoid the vagueness of definition of distance, and more importantly to capture the overall geometrical effect of varying the super offset while fixing the separation.

E. Array 5: Guard Ring Structures

One major application of the proposed compact model is in guard ring structures. Proper deployment and clean voltage biasing of guard rings can directly help enhance the sensitive circuits' immunity to the substrate noise, especially in a lightly doped process. Hence, guard ring structures are included in Array 5.

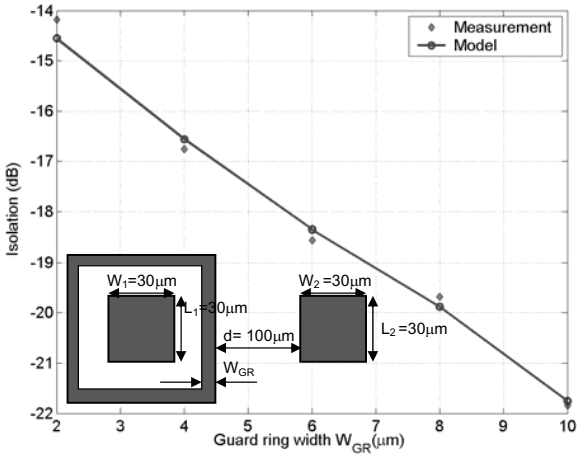

Fig. 14. Noise isolation sensitivity of guard ring size

Fig. 14 shows a typical guard ring protection configuration. The substrate noise isolation in dB is defined as

$$Isolation = 20\log_{10}\left(\frac{V_{victim}}{V_{aggressor}}\right) \quad (3)$$

The noise isolation sensitivity is shown in Fig. 14 with both

measurement data and modeling results. As can be seen from the plot, the noise isolation in dB is roughly proportional to the guard ring width W_{GR}, in other words, guard ring size. In this particular case, every 2 μm increase in guard ring width gains about 2 dB more noise isolation. Notice that the proposed model gives a very good prediction comparing to the measurement results.

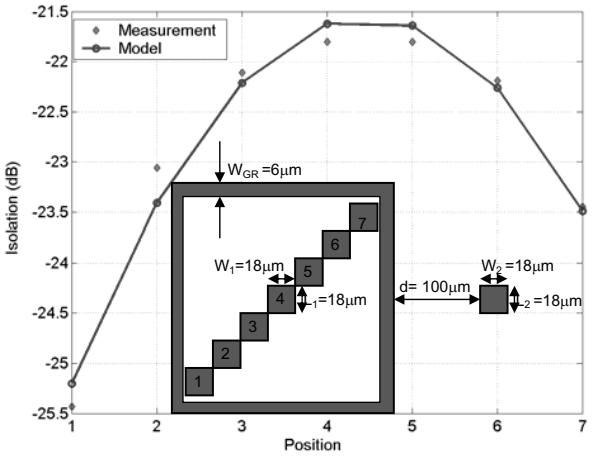

Fig. 15. Noise isolation sensitivity of noise victim's location inside guard ring

The layout shown in Fig. 15 studies how the positioning of a noise victim inside a guard ring can affect the noise isolation. The noise victim is placed in position 1 to 7, as labeled in the figure. The measurement data is shown in the same figure. It can be seen that the noise isolation degrades as the victim moves from position 1 towards position 4. This is obviously as expected because during this process a major factor is that the distance between the victim and aggressor decreases. However, it is more interesting to see that the noise isolation actually enhances as the victim continues to move from position 4 to position 7, by an improvement of 2 dB in this particular case. During this process the competing factor to the decreasing spacing between victim and aggressor is the closer and closer distance from the victim to the guard ring wall. This observation provides a practical design trade-off when the placement of sensitive circuitry inside a guard ring is explored. Note that the compact model again gives a good prediction of the isolation behavior.

V. Conclusions

In this paper, a synthesized compact model for substrate resistance in lightly doped processes has been presented. Far field and near field effects are recognized through device simulation. Geometrical parameters of substrate contact are included in the proposed model. A test chip using a lightly doped process has been fabricated. With fitting coefficients extracted from benchmark device simulation results and calibrated by the measurement, the model is verified by the measurement data from the test chip with error typically less than 5%. The method should be useful in fast model generation to facilitate the efficient substrate noise analysis in mixed-signal design.

Acknowledgements

This work was supported by DARPA under the NeoCAD project.

References

[1] N. K. Verghese and D. J. Allstot, "Computer-aided design consideration for mixed-signal coupling in RF integrated circuits," *IEEE J. Solid-State Circuits*, vol. 33, no. 3, pp. 314-323, Mar. 1998.

[2] E. Charbon, R. Gharpurey, R.G. Meyer, and A. Sangiovanni-Vincentelli, "Substrate optimization based on semi-analytical techniques," *IEEE Trans. Computer-Aided Design,* vol. 18, no. 2, pp. 172-190, Feb. 1999.

[3] M. Badaroglu, M. van Heijningen, V. Gravot, J. Compiet, S. Donnay, G. E. Gielen, and H. J. De Man, "Methodology and experimental verification for substrate noise reduction in CMOS mixed-signal ICs with syncronous digital circuits," *IEEE J. Solid-State Circuits*, vol. 37, no. 11, pp. 1383-1395, Nov. 2002, pp. 124-129.

[4] E. Schrik and N.P. van der Meijs, "Combined BEM/FEM substrate resistance modeling," *Proc. Design Automation Conf.,* New Orleans, Louisiana, June 10-14, 2002.

[5] S. Kristiansson, S. Kagganti, T. Ewert, F. Ingvarson, J. Olsson and K. Jeppson, "Substrate Resistance Modeling for Noise Coupling Analysis", *Proc. ICMTS*, June 2003.

[6] D. Ozis, T. Fiez, and K. Mayaram, "A comprehensive geometry-dependent macromodel for substrate noise coupling in heavily doped CMOS processes," *Proc. IEEE Custom Integrated Circuits Conf.,* Orlando, Florida, May 12-15, 2002, pp. 497-500.

[7] H. Lan and R. Dutton, "Synthesized Compact Models (SCM) of Substrate Noise Coupling Analysis and Synthesis in Mixed-Signal ICs", *Proc. Design, Automation, and Test in Europe Conf.*, Paris, France, Feb. 16-20, 2004, pp. 836-841.

[8] DAVINCI, Synopsys Inc., Mountain View, CA.

[9] F. Grover, *Inductance Calculations, Working Formulas and Tables*, D. Van Nostrand Company Inc., New York, 1946.

[10] TSUPREM, Synopsys Inc., Mountain View, CA

[11] H. Lan, Z. Yu, and R. W. Dutton, "A CAD-oriented modeling approach of frequency-dependent behavior of substrate noise coupling for mixed-signal IC design," *Proc. International Symposium on Quality Electronic Design*, San Jose, CA, Mar. 24-27, 2003, pp.195-200.